Journal of Non-Crystalline Solids 511 (2019) 86–99

Contents lists available at ScienceDirect

Journal of Non-Crystalline Solids

journal homepage: www.elsevier.com/locate/jnoncrysol

Influence of zinc ions on structure, bioactivity, biocompatibility and antibacterial potential of melt-derived and gel-derived glasses from CaO-SiO_2 system

Aleksandra Wajda[a,*], Wolfgang H. Goldmann[b], Rainer Detsch[c], Aldo R. Boccaccini[c], Maciej Sitarz[a]

[a] Faculty of Materials Science and Ceramics, AGH University of Science and Technology, Mickiewicza 30, 30-059 Cracow, Poland
[b] Deptartment of Physics, Biophysics Group, University of Erlangen-Nuremberg, 91052 Erlangen, Germany
[c] Institute of Biomaterials, Department of Materials Science and Engineering, University of Erlangen-Nuremberg, 91058 Erlangen, Germany

ARTICLE INFO

Keywords:
Bioactive silicate glasses
Spectroscopic studies
Zinc oxide
Biocompatibility
Antibacterial properties

ABSTRACT

Several different compositions of zinc-containing glasses in the CaO-SiO_2 system were obtained by both traditional melting technique and the sol-gel method. The influence of zinc ions addition in the glass composition was evaluated using different spectroscopic methods (FTIR and ^{29}Si MAS-NMR). It was demonstrated that ZnO has a significant effect on glass structure and, as a consequence, on thermal properties, texture and bioactivity. EDX and ICP data showed that zinc ions reduce glass bioactivity and incorporate in the newly forming HCA layer. Evaluation of the in vitro biocompatibility of the obtained materials was performed by indirect tests using MG-63 osteoblast-like cells. All samples were found to be biocompatible and zinc ions enhanced the cell viability. Antibacterial tests against gram-negative (*E. coli*) and gram-positive bacteria (*S. aureus*) were carried out to evaluate the antibacterial potential of the zinc-doped glasses.

1. Introduction

Silicate bioactive glasses are a widely used group of amorphous inorganic biomaterials. They are very desirable due to their ability to create strong chemical bonds with surrounding living tissues. This is done via hydroxycarbonate apatite (HCA) layer formed spontaneously on their surface in contact with physiological fluids [1]. Silicate alkali-free glasses are well-known from their reduced crystallization tendency, lower susceptibility to water uptake and decreased coefficient of thermal expansion [2]. There are many studies on glasses from CaO-SiO_2 system, which have proved their bioactive properties and biocompatibility, despite lack of phosphorous and alkali [3–7]. Bioactive glasses are mainly used in hard tissue regenerative medicine as bone grafts or fillers in the field of bone and teeth repair [8]. One of the major advantages of these materials is the facile incorporation of different ions in the silicate matrix in order to improve their mechanical, physical and therapeutic properties. The release of dopant ions can enhance bioactivity, improve biological response of cells (e.g. osteogenesis and angiogenesis) and introduce antibacterial activity [9] [10]. To model and predict the behavior of bioactive glasses, it is essential to know the influence of different ions on glass structure, which plays a key role in determining the glasses' properties.

The choice of zinc ion addition was determined due to many literature reports, which inform that glasses containing ZnO can be considered chemically stable, non-toxic, biocompatible and with a good activity against *E. coli*, *S. aureus*, *C. krusei, B. subtilis* and *P. aeruginosa* [11–13]. At the same time, it is worth to mention that some of the authors reported that too high level of zinc concentration can be cytotoxic to osteoblast cells [14]. However, it is difficult to clearly indicate the limit value of zinc in the glass composition, which causes cytotoxicity because it may be dependent on many factors, including cell line, synthesis routes and related glass microstructure, surface morphology, zinc release kinetics, etc. [14] [15].

Zinc ions in silicate glass structure act both as network modifiers and network formers.[3] The role of ZnO can switch from being a network modifier to being an intermediate oxide by increasing the ZnO content [9]. Formation of the tetrahedral ZnO_4^{2-} species requires Ca^{2+} ions for charge balancing. This can lead to cations removal from the silicate network, inducing formation of the Si-O(Zn) bonds and, as a consequence, an increasing of the number of bridging oxygen (BO) species. Despite the fact that the polymerization level is increased, the presence of the Si-O(Zn) bonds that are weaker than Si-O-Si bonds can weaken

* Corresponding author.
E-mail address: olawajda@agh.edu.pl (A. Wajda).

https://doi.org/10.1016/j.jnoncrysol.2018.12.040
Received 28 September 2018; Received in revised form 28 December 2018; Accepted 31 December 2018
0022-3093/ © 2019 Elsevier B.V. All rights reserved.

the glass network causing a reduction of the glass transition temperature [16].

Analysis of the available literature indicates that it is difficult to unequivocally define if Zn^{2+} ions improve or inhibit glass bioactivity and biocompatibility because different studies have not been carried out on the same composition of glasses, and the glasses have been obtained in a different ways [16]. Thus, further specific studies on the relationship between the structure, microstructure, physicochemical properties, and mode of synthesis are required to accurately determine the influence of zinc ions on the dissolution rate, bioactive and biocompatible behavior of zinc-doped glasses [10].

In this study, a selection of zinc containing silicate glasses was investigated and Zn content was related to its important role in formation and metabolism of bone cells [17], growth of blood vessels [18], wound healing [19] [20], as well as its antibacterial properties. According to the literature [21], depending on the condition, Zn^{2+} can be either bacteriostatic or bactericidal. Bacteriostatic effect is achieved by inhibition of the glycolysis processes. Meanwhile, bactericidal properties originate from the semi conductive nature of the ZnO, which may induce formation of free radicals and the intrinsic ability of ZnO to cause distortion in bacteria cells' membranes [22].

Thus, the aim of this work was to describe the effect of zinc ion addition in silicate glasses on the structure of both gel-derived and melt-derived glasses from CaO-SiO_2 binary system. It was expected that ZnO addition, as well the processing method, will have an impact on the glass structure, thermal properties, texture and solubility. As these qualities are known to have an impact on the bioactivity, biocompatibility and antibacterial properties of the biomaterials, different reactions in vitro were expected for the ZnO-doped glasses, as compared to standard CaO-SiO_2 binary system.

2. Materials and methods

2.1. Preparation of the glasses

Gel-derived and melt-derived glasses from the ZnO-CaO-SiO_2 system were obtained in order to compare the impact of the fabrication method on some of the basic properties. Table 1 shows the assumed chemical composition of the obtained materials and the corresponding nomenclature used throughout the paper.

Gel-derived glasses were synthesized using sol-gel method as described by Vallet-Regi et al. [5]. Synthesis of the ZnO-CaO-SiO_2 glasses was performed with the following reagents: tetraethoxysilane (TEOS, $Si(OC_2H_5)_4$), calcium nitrate tetra-hydrate($Ca(NO_3)_2{\cdot}4H_2O$), zinc nitrate hexahydrate ($Zn(NO_3)_2{\cdot}6H_2O$), 2 N nitric acid (HNO_3) and distilled water. During preparation, the HNO_3 amount was dependent on the molar ratio of H_2O to TEOS (=8). The aim of synthesis was to obtain homogeneous solutions, which required 14 days of drying at room temperature. Then, the obtained gels were dried at 120 °C for 24 h and further at 700 °C for 3 h (heating ramp 10 h), according to the previous research [23].

Glasses with the same oxide composition as the gel-derived ones (presented in Table 1). were obtained by traditional melting technique. The appropriate amounts of silicon dioxide (SiO_2), calcium carbonate ($CaCO_3$) and zinc oxide (ZnO) were mixed in a mortar. Afterwards, homogeneous mixtures of powder were melted in the electric furnace in a platinum crucible at 1730 °C for 2 h. All gel-derived and melt-derived glasses were milled and homogenized in an agar mortar and sieved to receive the glass powders with particles size lower than 45 μm used in all of the experiments. The chemical compositions of the obtained glasses were confirmed by the X-ray Fluorescence Spectrometry (XRF) method, using a WD-XRF Axios Max spectrometer with Rh 4 kW PANalytical lamp. The differences between theoretical composition and experimental, as measured by XRF, were in all cases lower than 6%.

Table 1
Nominal chemical composition of glasses.

Sample name	% mol SiO_2	% mol CaO	% mol ZnO	Processing method
70S30C_m	70	30	0	melt-derived
2Zn_m	70	28	2	
4Zn_m	70	26	4	
70S30C_sg	70	30	0	sol-gel synthesis
2Zn_sg	70	28	2	
4Zn_sg	70	26	4	

2.2. X-ray diffraction (XRD) and morphological characterization

A Philips/Panalytical X'Pert Pro MD powder diffractometer using Cu Kα1 radiation was used to analyze all powders. Standard Bragg-Brentano geometry with Θ-2Θ setup was applied (0.008° step size and 5°-90° 2Θ range).

Morphologies of the obtained glass powders and newly formed HCA layers were observed by scanning electron microscopy (Nova NanoSEM 200, FEI Europe Company). Before the observation, all glass powder samples were coated with a thin layer of carbon to avoid charge accumulations at the surface of the samples, which leads to formation of noise.

Due to high specific surface area (> 100 m^2/g) of the gel-derived glasses, additional evaluation of their texture and porosity was necessary. These were done using a Micromeritics ASAP 2000 and evaluation of N_2 physisorption using the BJH (Barrett, Joyner and Halenda) model of desorption branch of the isotherm, respectively.

2.3. FTIR spectroscopy

A Bruker Optics-Vertex70V spectrometer was used to perform FTIR studies of the materials. Samples were prepared as standard KBr pellets. The spectra were collected in the 4000–400 cm^{-1} range, averaged from 128 scans, and with 4 cm^{-1} resolution.

Spectra deconvolution was done via OPUS software, according to the method of Handke et al. [24]. A mixed Gaussian/Lorentians function was used to provide a good quality fitting for complex band envelopes. The residual root-mean-square (RMS) error for IR deconvolution was < 0.003.

2.4. MAS-NMR spectroscopy

The ^{29}Si solid state MAS-NMR spectra were measured on the APOLLO console (Tecmag) at the magnetic field of 7.05 T provided by the 300 MHz/89 mm superconducting magnet (Magnex). A Bruker HP-WB high-speed MAS probe equipped with the 4 mm zirconia rotor and KEL-F cap was used to spin the sample at 4 kHz. The resonance frequency was equal to 59.515 MHz, and a single 3 μs rf excitation pulse corresponding to a π/2 flipping angle was applied. The number of averages was 512, with the acquisition delay equal to 60 s. The frequency scale in ppm was referenced to TMS (tetra-methylo-silane). Curve fitting procedure was done using Bruker OPUS 7.2 software and in accordance with a method proposed by Handke M. et al. [24]. Spectra RMS error was found to be lower than 0.20.

2.5. Thermal properties

DSC (differential scanning calorimetry) curves were recorded with the aid of a simultaneous thermal analyzer (STA 449 F1 Jupiter, Netzsch company). The samples were placed in platinum crucibles and heated to 1100 °C at a rate of 10 °C/min under a protective flow of nitrogen. Data evaluation was performed on Netzsch Proteus Thermal Analysis software and was aimed at evaluating the glass stability and glass transition temperatures.

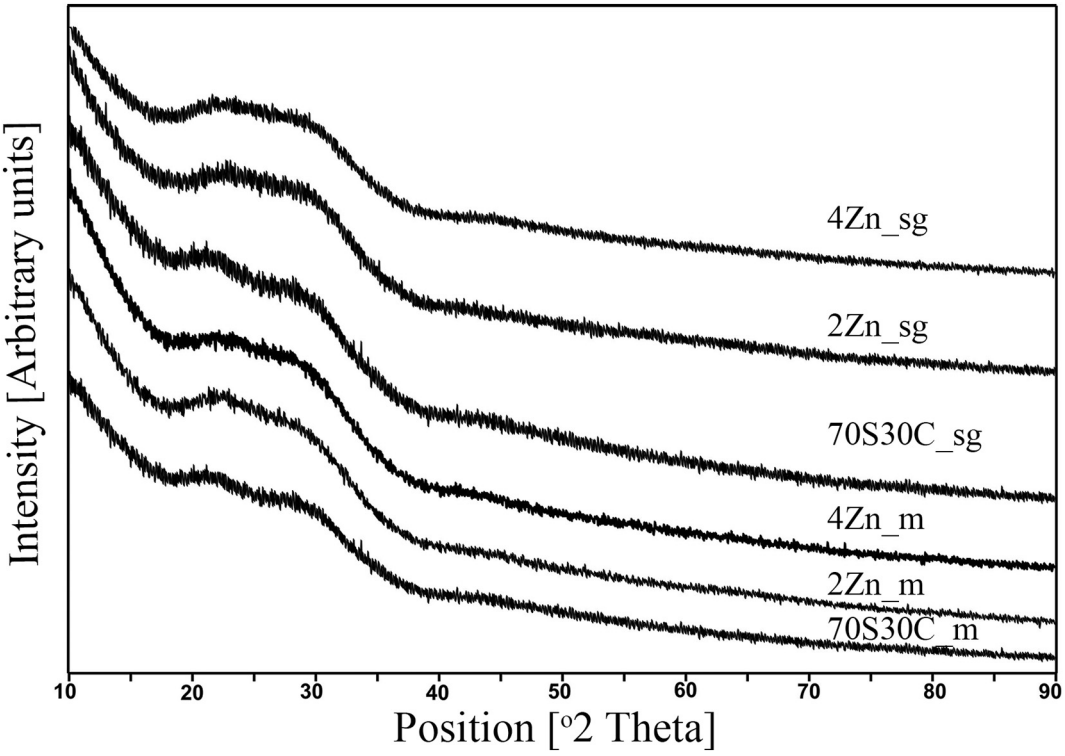


Fig. 1. XRD of the obtained samples (see Table 1).

2.6. Ion release and bioactivity tests

Bioactivity studies were performed in accordance with a standardized protocol by Kokubo and Takadama and the Simulated Body Fluid (SBF) was prepared following the provided recipe [25]. Each glass powder (< 45 μm) was immersed in distilled water at a ratio of 0.1 g of glass to 10 ml of distilled water and in the SBF at a ratio of 75 mg of glass to 50 ml of SBF. The powders were incubated for 24 h, 1 week, 2 and 3 weeks at 37 °C. The changes of pH values of the filtered solutions were measured and ion concentrations were determined using inductively coupled plasma optical emission spectrometry (ICP-OES; Plasma 40, Perkin Elmer, USA). Distilled water and SBF were used as a control. The following uncertainties for individual elements: Ca – 6.07%, P-6.78%, Si-6.45%, Zn-6.18% are declared in ICP-OES measurements.

Formation of calcium phosphate apatite-like layers on the surface of the glass powders after different soaking times in SBF was observed by SEM and FTIR measurements were performed to identify the type of crystallized phase.

2.7. Test of in vitro biocompatibility

The samples were sterilized in a furnace at 160 °C for 2 h. Afterwards, sterile samples were placed in DMEM (Dulbecco's modified Eagle's medium, Gibco, Germany) at a ratio of 0.1 g glass to 10 ml (1% wt/vol) DMEM in plastic tubes. Afterwards, the powders were incubated for 24 h at 37 °C, in a 5% CO_2 enriched, humidified atmosphere. The extracts were diluted with additional medium to produce extracts at 0.1% and 0.01% (wt/vol).

Osteoblast-like (MG-63) cells (Human osteosarcoma cell line, Sigma-Aldrich) were placed in 24-well plates (at a count of 100,000 cells/well) and incubated for 48 h with glass extracts obtained by pre-incubating.

Cellular viability was characterized by mitochondrial activity measurements using the WST-8 (Sigma-Aldrich) assay. The test was performed according to the manufacturer's protocol after 48 h of culture. The absorbance was measured with single-beam spectrophotometer (Specord 40, Analytic Jena) at 450 nm.

The number of cells attached to the wells was established by measuring the LDH enzyme activity in the cell lysate. This was done using a commercially available LDH-activity quantification kit (TOX7, Sigma-Aldrich). The test was performed according to the manufacturer's protocol after 48 h of culture. The primary wavelength measurements were done at 490 nm from which the background absorbance was subtracted (measured at 690 nm).

To investigate the cell morphology, adherent growth, and distribution, cells were fixed with buffered paraformaldehyde in PBS and stained with hematoxylin and eosin. Then, the samples were observed under an inverted light microscope (Zeiss, Primovert).

2.8. Antibacterial studies

Investigation of the antibacterial properties of zinc-containing glasses was carried out using gram-negative (*E. coli*) and gram-positive bacteria (*S. aureus*). The sterile samples were placed in LB Medium (Carl Roth GmbH, Karlsruhe, Germany) at a ratio of 0.1 g glass to 10 ml LB Medium in plastic tubes. The powders were placed in an incubator at 37 °C for 24 h to get medium-sample extracts. The bacteria were taken from a colony of bacteria and mixed with 5 ml of LB medium. The bacterial cells were placed in the incubator overnight at 37 °C for growth. Thereafter, the solution was diluted to obtain an optical density OD_{600nm} of approx. 0.015 (Biophotometer, Hamburg, Germany). Two types of experiments were done using a different ratio of medium-sample extract to bacteria mixture (1 ml:0.5 ml or 1 ml:0.2 ml). 1 ml of medium-sample extracts were pipetted into Eppendorf tubes (3 replicas of each sample). Then, 0.5 ml/0.2 ml of obtained bacteria mixture were added to each tube. The reference was 1 ml of LB medium and 0.5/0.2 ml of bacteria mixture. The optical density of all samples were measured and compared with the reference. The percentage decrease of bacteria was calculated.

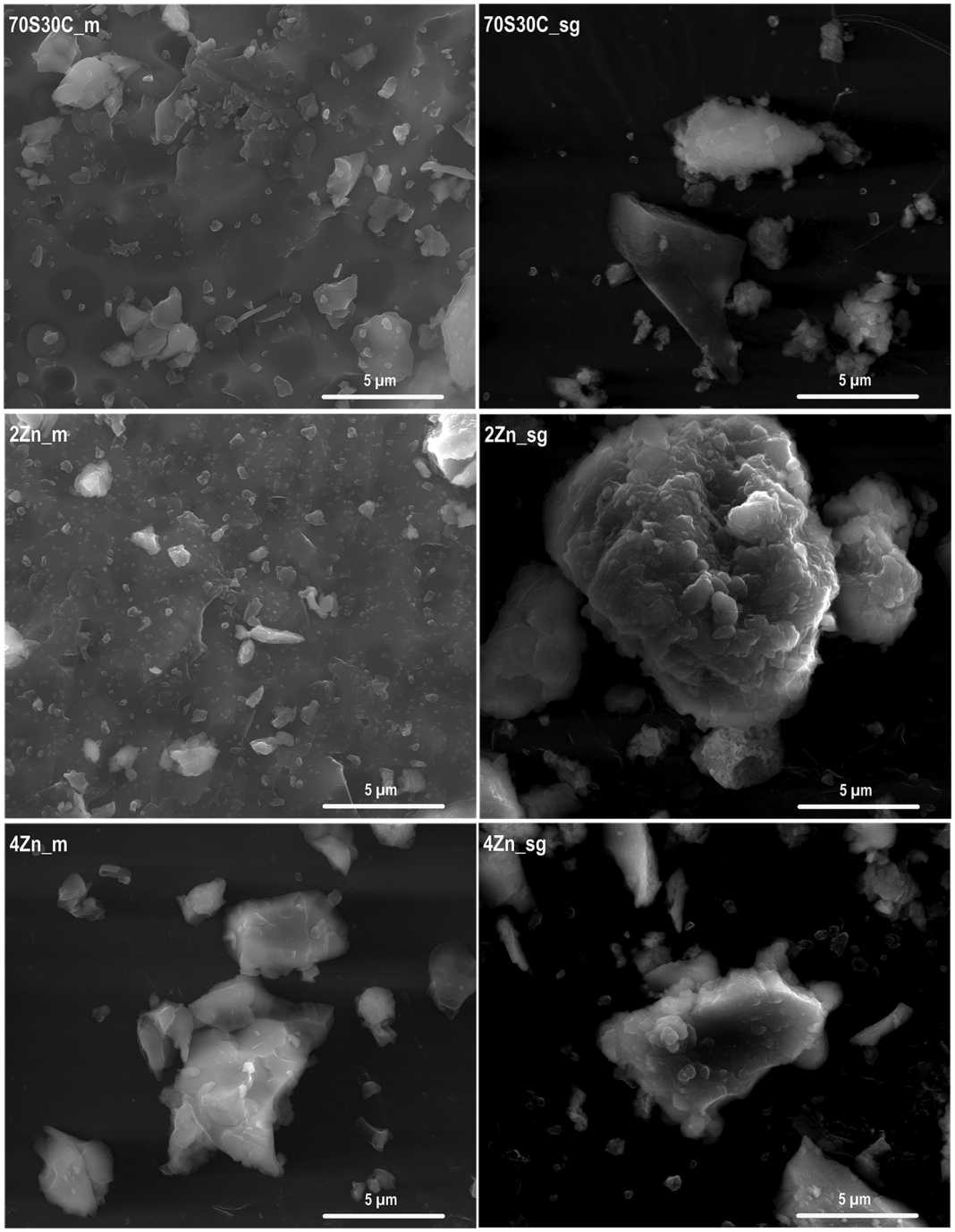


Fig. 2. SEM microphotographs of obtained glasses.

2.9. Statistical analysis

Results for WST-8, LDH and antibacterial test are shown in bar charts representing the mean value ± standard deviation. The differences between experimental groups were compared by one-way analysis of variance (ANOVA). The level of the statistical significance was defined at $p < .05$ (OriginPro 8.5, OriginLab Corporations, USA).

3. Results and discussion

3.1. X-ray diffraction and morphological characterization

To confirm the amorphous state of all the obtained materials, XRD diffractograms were obtained. In the XRD patterns (Fig. 1) no reflections can be seen, thus confirming the amorphous state of all of the prepared materials. In the XRD diagrams of 70S30C glasses, there can be seen two adjoined large maxima (so-called two amorphous halos), which can be associated with phase separation.

A scanning electron microscope (SEM) analysis was performed on the obtained glasses to investigate their microstructure (Fig. 2). In case of 70S30C_m and 2Zn_m glasses, phase separation can be observed. There are visible glassy spherical inclusions in a glassy matrix. It appears that the chemical composition of the inclusions should be different from the chemical composition of the matrix, but the inclusion size was found to be too small to perform EDX analysis. Addition of zinc ions caused significant homogenization of the melt-derived glass

Table 2
Data of the gel-derived glasses powder characterization.

Sample	BET specific surface area [m^2/g]	BJH specific pore volume [g/cm^3]	BJH average pore diameter [nm]
70S30C_sg	136.81 ± 0.32	0.4107 ± 0.0020	8.58 ± 0.25
2Zn_sg	108.62 ± 0.24	0.2150 ± 0.0011	5.52 ± 0.14
4Zn_sg	122.01 ± 0.21	0.2041 ± 0.0016	4.66 ± 0.18

microstructure; the inclusions in the 2Zn_m glass were less noticeable and in case of 4Zn_m, they were not found. Based on the diffractograms, it can be seen that the addition of zinc resulted in two separate maxima being less visible, what can confirm microstructural homogenizing influence of zinc on glass microstructure. The gel-derived glasses seem to have more homogeneous microstructure, higher surface area and surface porosity.

Phase separation in glasses takes place because of the thermodynamic non-ideality. A system can reduce its free energy by separating into two or more phases. This phenomenon is associated with an excess free energy [26].

Based on Table 2, which presents BET specific surface area, specific pore volume and specific pore diameter values as a function of the composition of the gel-derived glasses, it can be noticed that the addition of Zn^{2+} ions has a significant effect on the glass texture. It is evident that the specific pore volume and the specific pore diameter decreased with increasing amount of zinc in the glass. Moreover, the zinc ions addition leads to the slight decrease the surface area.

The incorporation of divalent ions (Zn^{2+}) may disrupt the ordered orientation of SiO_4^{4-} during the self-assembly reaction, what may lead to appearance of additional structural defects in the atomic array and further change of pores shape and structure [12]. The changes in textural characterization of these powders may have an influence on ions release and bioactivity.

The differences in specific surface area and porosity between gel-derived and melt-derived glasses were presented in previous article [27]. In case of material with low surface area, it was not possible to designate specific pore volume and average pore diameter.

3.2. FTIR spectroscopy

The influence of zinc ions as well as fabrication methods on the glass structure were evaluated by Mid-infrared (MIR) spectroscopic studies.

Fig. 3 shows MIR spectra of all of the obtained glasses and their spectra deconvolution. Deconvolution into component bands allowed for a more precise interpretation of overlapping bands. It can be seen that both the fabrication method and presence of the zinc ions have a substantial effect on the degree of polymerization of the silicate network. The most noticeable differences between spectra can be observed in the range of 1300–800 cm^{-1}, associated with asymmetric stretching vibrations of Si═O (defects), Si-O(Si) and Si—O^- [28–30] [4].

In a previous paper, it was demonstrated that gel-derived glass from the CaO-SiO_2 system had a more polymerized structure as compared with melt-derived glass with the same chemical composition [27]. To manifest it, the ratio of the NBO (non-bridging oxygen) integral intensity to the sum of the BO integral intensity was calculated. The bands associated with the NBO are located at about 920-910 cm^{-1} (asymmetric stretching Si—O— vibrations) and the bands assigned to the BO (asymmetric stretching Si-O(Si) vibrations) are in the range between 1110 and 1030 cm^{-1} (Fig.3) [4] [28–30].

The same analysis of zinc-doped glass spectra can demonstrate similar tendency (regardless of the content of zinc ions). In case of the melt-derived glasses with zinc ions, the above-mentioned ratio of integral intensity is much higher in comparison with the gel-derived ones (Table 3). This result indicates that glasses obtained by sol-gel synthesis have higher level of network polymerization.

The executed deconvolution of the MIR spectra permitted evaluation of the influence of Zn^{2+} ions on the structure of the as-obtained glasses. The addition of Zn^{2+} causes the intensity increase of the band associated with non-bridging oxygen Si—O^- at about 920–910 cm^{-1} and thus it results in the decrease of the intensity of bands connected with bridging oxygen Si-O(Si) (at 1115–1020 cm^{-1}). The above described ratio of integral intensity Si-O^-/Si-O(Si) for zinc doped glasses may indicate that zinc ions play a role as network modifiers (they occur in octahedral coordination geometry, coordination number 6).

In the deconvoluted MIR spectra of the gel-derived glasses, two additional bands at about 1700 and 1630 cm^{-1} are visible. According to the literature, the bands at about 1630 cm^{-1} originate from H-O-H bending vibrations of the water molecules [4], while the 1700 cm^{-1} bands are related to C═O stretching vibrations, what indicates the presence of residual carbonate groups in the glass structure [31]. Presence of these bands in the spectra should be associated with the applied method of glass synthesis but may also arise from the material's significant porosity, being favorable for water adsorption. In all spectra, the bands positioned at 1204–1244 cm^{-1} can be assigned to the Si═O vibrations (defects) [30] [32].

It can be stated that the introduction of zinc ions into the structure of glasses from the CaO-SiO_2 system, regardless of the method of its preparation, leads to depolymerization of the silicate network. This effect might be explained by homogenizing influence of zinc ions on glass microstructure causing an increase of non-bridging oxygen and it may indicate that ZnO can disrupt the glass network more efficient than CaO.

3.3. ^{29}Si MAS-NMR spectroscopy

^{29}Si MAS-NMR studies were employed to confirm the results obtained from the FTIR and the measured spectra are presented in Fig. 4.

It can be seen that in both types of glasses, the addition of zinc ions causes the appearance of Q units with a lower value (bands are shifted to higher ppm) compared with the basic glass 70S30C [33]. It undoubtedly indicates that zinc ions act as modifiers of the glass network, i.e., they occur in coordination number (CN) 6. It should also be noticed that in the case of melt-derived glasses, small amounts of the Q^3 units appeared (bands at lower ppm). It may indicate that some of the zinc ions are also network formers, i.e., they occur in tetrahedral coordination (CN = 4). A similar situation is observed in the case of gel-derived glasses. The introduction of zinc ions leads to an intensity increase of bands associated with Q^4 units (in comparison to the base glass) indicating the presence of some of the zinc ions in tetrahedral coordination. The appearance of two different Q^2 and Q^4 units in the zinc-doped glasses can confirm the presence of two vibration types associated with Si-O-Si and Si-O-Zn. Table 4 presents information about the types of Q units and their relative contributions calculated based on NMR spectra.

MAS NMR analysis on zinc nuclei would be conclusive in this case. However, it was found to be impossible to register spectra of good quality because of too low content of zinc ions in the glasses. Therefore, only in the presented (indirect) way, was it possible to determine the role of zinc ions in glasses from the CaO-SiO_2 system.

3.4. Thermal analysis

To examine the influence of Zn^{2+} on characteristic temperatures and the thermal stability of the glasses, DSC measurements were performed (Fig. 5). Two-step crystallization is proven by the presence of two separate exothermal peaks visible on DSC curves of both glasses. It means that likely two phases are present in the structure (as revealed via SEM investigations; namely matrix and inclusions), which can crystallize separately at different temperatures [34] [35]. The addition of zinc ions was found to change the character of the DSC curves. Crystallization occurred in one stage (only one exothermal peak is

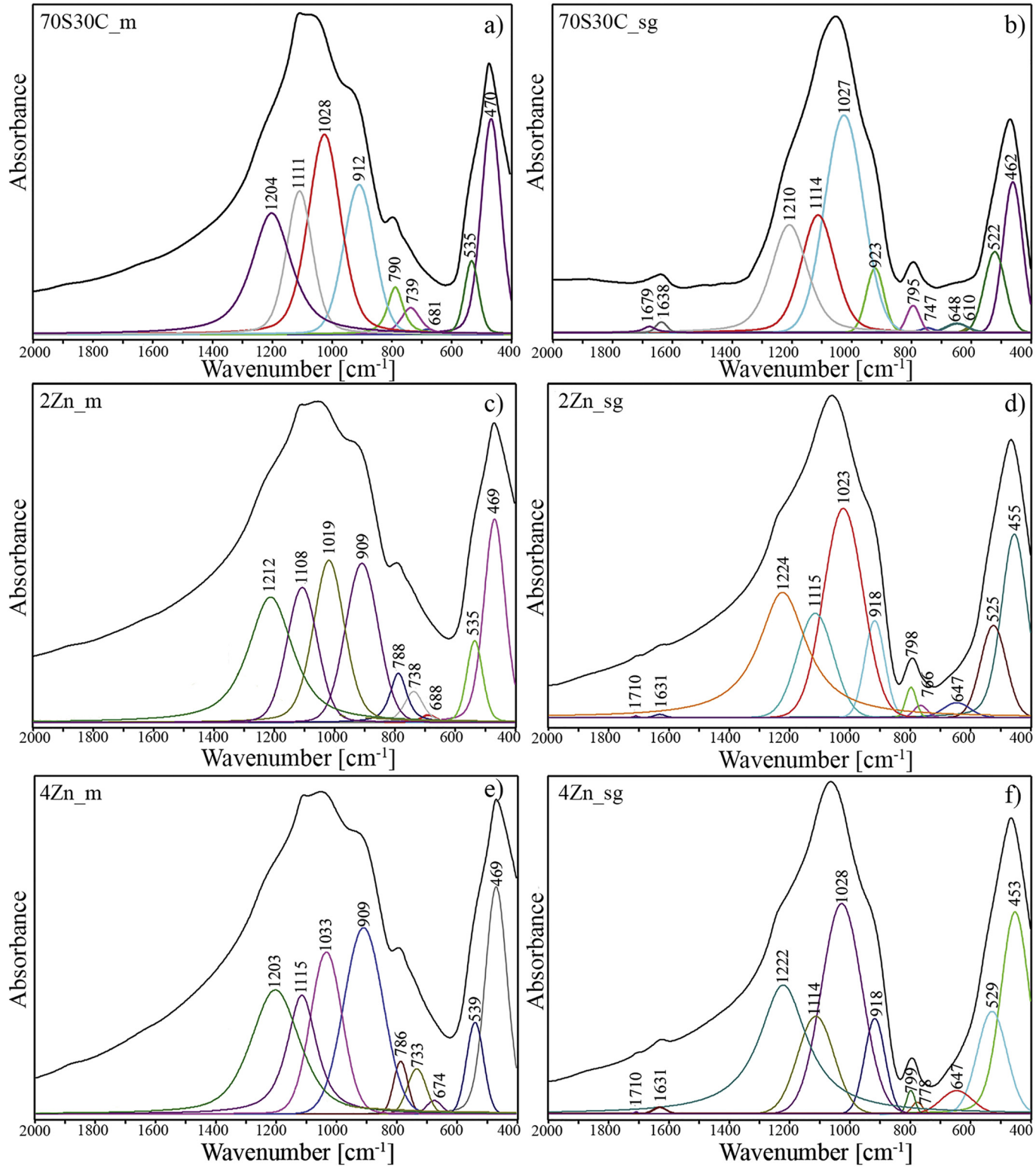


Fig. 3. Deconvolution of the MIR spectra showing the differences in the ratio of integral intensity NBO/BO: a) 70S30C_m, b) 70S30C_sg, c) 2Zn_m, d) 2Zn_sg, e) 4Zn_m, f) 4Zn_sg.

visible), and a shift towards lower temperatures was observed. This may confirm that glasses from the ZnO-CaO-SiO_2 system have a more homogenous microstructure (no clear phase separation) than glasses from CaO-SiO_2 system.

The values for the glass transition temperatures (T_g) are given in Table 5. Comparing Tg of the 70S30C glasses with zinc-doped ones, a decrease of T_g with an increasing amount of ZnO is observed. Changes in the T_g values may be explained by a weakened network of zinc-doped glasses through depolymerization of glass network along with the creation of Si-O(Zn) bonds (as confirmed via FTIR and NMR_MAS). As reported in literature, the presence of Zn^{2+} in the role of both network modifier and the values of T_g for all of the gel-derived glasses are higher

Table 3
Comaprison of integral intesity ratio.

Sample	Ratio of integral intensity Si-O$^-$/Si-O(Si)	Sample	Ratio of integral intensity Si-O$^-$/Si-O(Si)
70S30C_m	0.41	70S30C_sg	0.09
2Zn_m	0.53	2Zn_sg	0.16
4Zn_m	0.72	4Zn_sg	0.16

than for melted ones which may originate from the higher polymerization level, as reveled by the structural evaluation (section 3.2 and 3.3) [36] [37].

3.5. Ions release

Release of Ca, Si and Zn ions from the glass structure was measured in DI water (Fig. 6) and it was found that the ion concentrations depended on the amount of zinc in the glass and on the fabrication method. In particular, the amounts of released Ca and Si ions were lower for zinc-doped glasses, which may be related to the double role of zinc in the glass structure and the microstructural changes demonstrated in Table 2 (zinc-doped glasses have lower surface area what may lead to lower ion release). It can be observed that the gel-derived glasses released higher amounts of these ions into the solution as compared with their melted equivalents, which can be explained by their higher surface area.

As expected, the release of zinc ions into the solution was proportional to the amount of zinc in the glass composition. When comparing two fabrication techniques, it was found that the melt-derived glasses release higher amounts of the Zn^{2+} ions than the gel-derived ones. The reason of this phenomenon may be the higher pH of the gel-derived glasses in solution (Fig. 7) and, as a consequence, the precipitation of $Zn(OH)_2$ (which is known to occur in basic solution) or the re-incorporation of zinc into the glass surface [38].

For most of the ZnO modified samples, the highest concentration of zinc ions was noticed after 24 h, while for the 2Zn_m glass, the maximum was observed after about 7 days.

3.6. Bioactivity tests

The evaluation of zinc influence on the bioactive properties of the all glasses was carried out in SBF solution. Fig. 7 shows the plots of

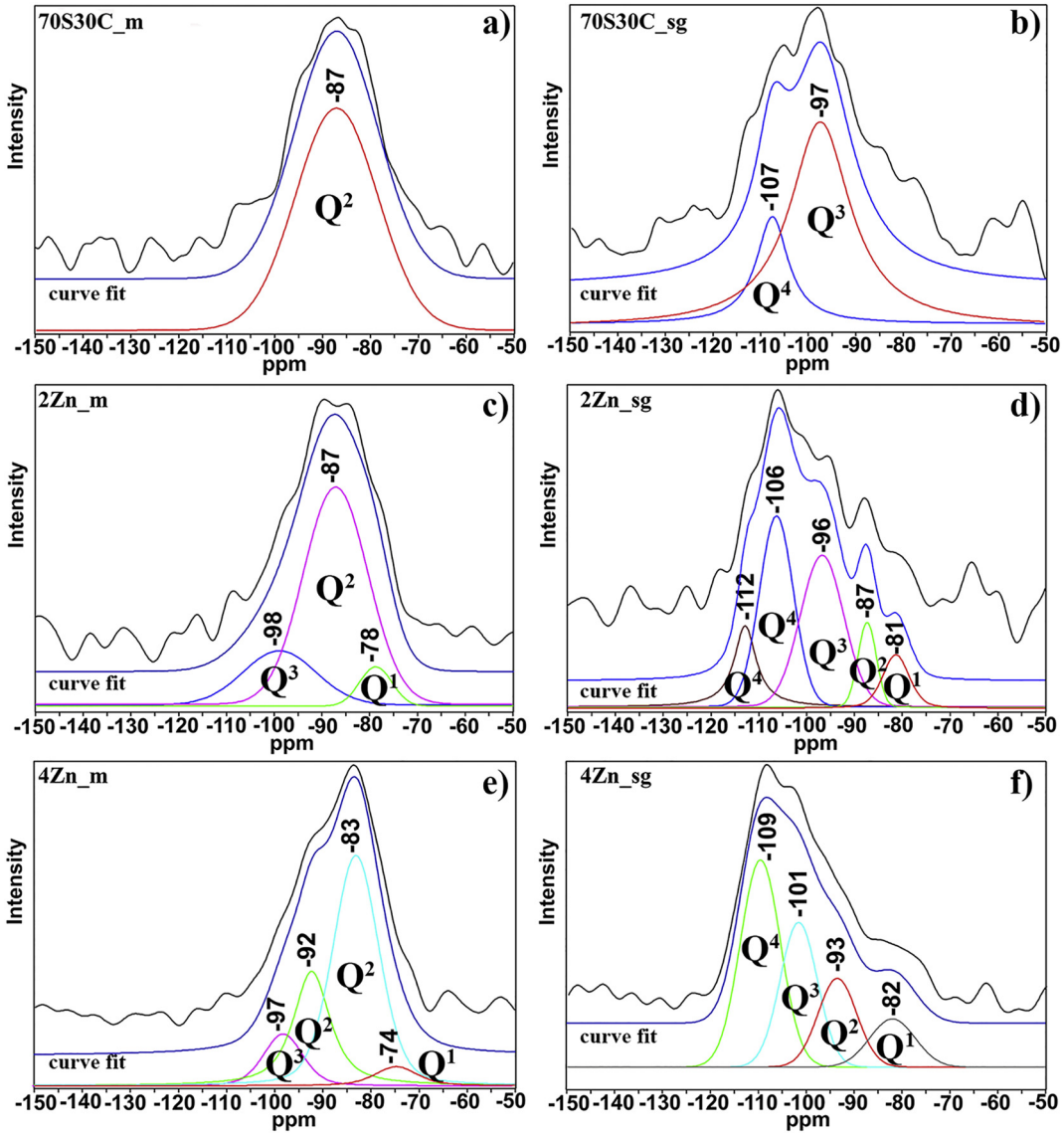


Fig. 4. ^{29}Si NMR MAS spectra and their deconvolution confirming double role of zinc ion in the glass structure: a) 70S30C_m, b) 70S30C_sg, c) 2Zn_m, d) 2Zn_sg, e) 4Zn_m, f) 4Zn_sg.

Table 4
Comparison of the relative contribution of the structural units in the synthesized glasses according to 29Si MAS NMR spectra (FWHM – full width at half maximum).

Sample	Chemical shift (ppm)	Relative contribution (%)	Type of structural unit	FWHM [ppm]
70S30C_m	−-87	100	Q^2	20.2
2Zn_m	−-78	7	Q^1	7.9
	−-87	72	Q^2	15.8
	−-98	21	Q^3	17.9
4Zn_m	−-74	5	Q^1	10.3
	−-83	57	Q^2	11.3
	−-92	27	Q^2	9
	−-97	11	Q^3	9.6
70S30C_sg	−-97	78	Q^3	15.4
	−-107	22	Q^4	8.8
2Zn_sg	−-81	9	Q^1	6.5
	−-87	8	Q^2	4.5
	−-96	35	Q^3	10.6
	−-106	34	Q^4	8.4
	−-112	14	Q^4	5.5
4Zn_sg	−-82	12	Q^1	11.1
	−-93	18	Q^2	9.5
	−-101	28	Q^3	9.1
	−-109	42	Q^4	9.8

ionic concentrations of Ca, P and Zn in SBF and the pH changes of the solution after different soaking times.

In all solutions, the highest increase of the Ca ions concentration and pH values was observed on the first day. The solutions' pH, initially 7.4, increased to 7.8 and to 8.2 for melt-derived glasses and gel-derived glasses, respectively. The increase of pH is most likely related to the exchange of ions between the glass and the solution (Ca^{2+} and H^+ respectively) [39] [40]. Higher pH values observed in the case of the gel-derived glasses are associated with the higher surface area of these glasses which leads to a higher calcium ions exchange. This behavior can also be related to the presence of the OH^- groups in the structure of this glass. A decrease of P concentration in SBF is observed for all glasses, and since P is involved in the formation of hydroxyapatite, the reduction rate of P concentration can be used to compare the rate of apatite formation between the bioactive glasses [41]. Comparing P concentration plots of melt-derived glasses, it can be suggested that the addition of Zn ions reduces the bioactivity of these glasses. The SBF solution of 70S30C_m glass contains < 3 ppm of phosphorus after 1 week, while P concentration of melt-derived zinc-doped glasses decreased to around 15 ppm and remained at this level.

In the case of gel-derived glasses, a reduction of bioactivity is observed only for 4Zn_sg glass. The plots of 70S30C_sg and 2Zn_sg have similar shapes and in both cases concentration of P reached a plateau of < 2 ppm after 7 days.

Table 5
The characteristic glass transition temperature (Tg) of the gel and melt-derived glasses.

Sample	Tg [°C]	Sample	Tg [°C]
70S30C_m	754	70S30C_sg	776
2Zn_m	746	2Zn_sg	757
4Zn_m	739	4Zn_sg	742

In general, the concentration of zinc increased on the first day, but remained at relatively low levels (< 0.14 ppm) throughout the experiment. An exception is the 2Zn_sg, which achieved its maximum concentration in 7 days. After reaching the maximum of Zn concentration, there was a sudden decrease in Zn concentration in solution. Comparing the zinc ions release into water (Fig. 6) to their release into the SBF (Fig. 7), it can be seen that there is a large difference between the maximum concentrations reached for each of the glasses. In water, the maximum zinc concentrations were between 0.8 and 0.1 ppm, while in the SBF solution, these values were around ten times lower. The fact that there is a decrease of release observed in the SBF solution can be explained by the depletion of released zinc ions by the occurrence of HCA surface precipitation reactions. The zinc ions can be partly incorporated into the forming HCA layer [42].

SEM microphotographs and EDX analysis of surfaces of the immersed samples were performed to precisely analyze the morphology and chemical composition of the newly formed layer. Fig. 8 demonstrates formation of small spherical aggregates of HCA covering surface of the immersed glasses. The EDX analysis (Fig. 9) confirmed that the chemical composition of the crystallized layer contains Ca and P ions. The presence of these elements suggests the formation of hydroxyapatite. Apart from that, in ZnO-modified glasses, the newly formed layer also exhibited peaks that can be assigned to the zinc ions. The intensity increase of the peaks is more visible after 3 weeks of incubation. These results may confirm that the decrease of Zn ions observed in the SBF solution after prolonged soaking may be associated with the fact that these ions are being incorporated into the forming HCA.

To confirm the type of newly formed layer on the surface of glasses, the FTIR spectra of the samples after 3 weeks of immersion in SBF was provided (Fig. 10).

In the spectra of 70S30C_m, 70S30C_sg and 2Zn_sg glasses, there can be seen characteristic band doublets at about 602 and 560–565 cm^{-1},

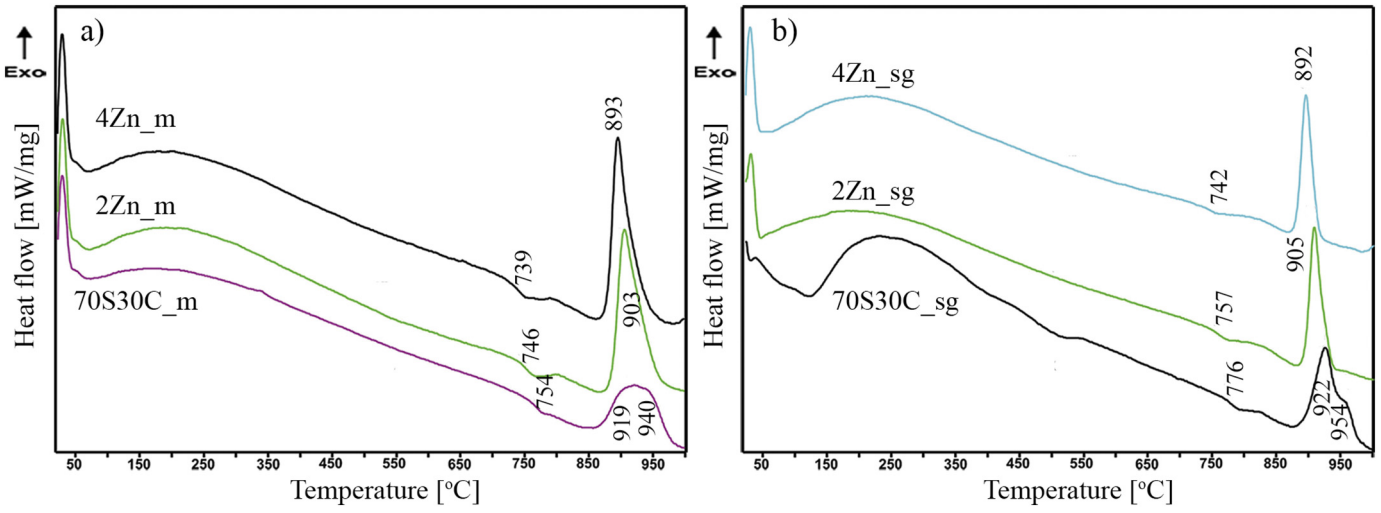


Fig. 5. DSC analysis showing the glass transition point and crystallization event: a) melt-derived glasses, b) gel-derived glasses.

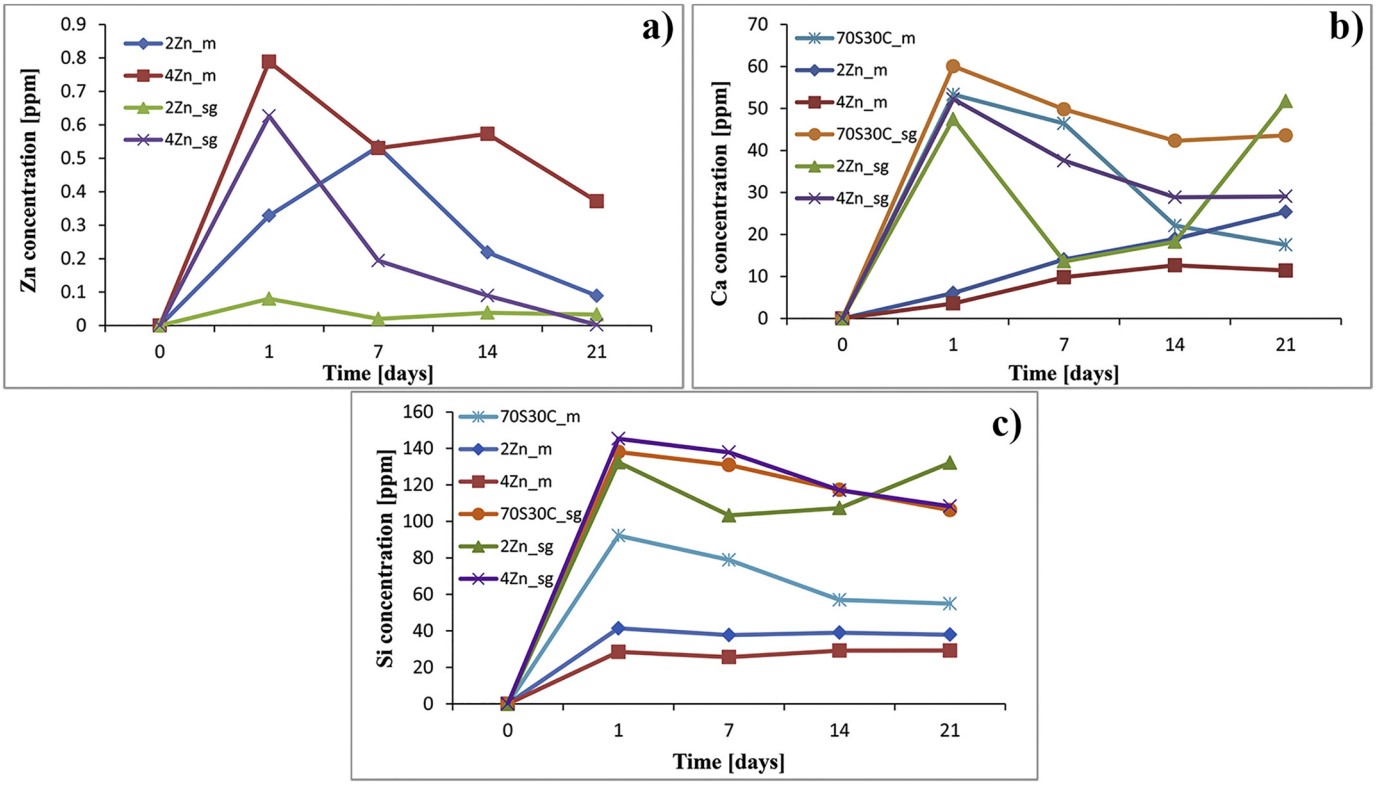


Fig. 6. Ions concentrations of samples in DI water: a) Zn, b) Ca and c) Si.

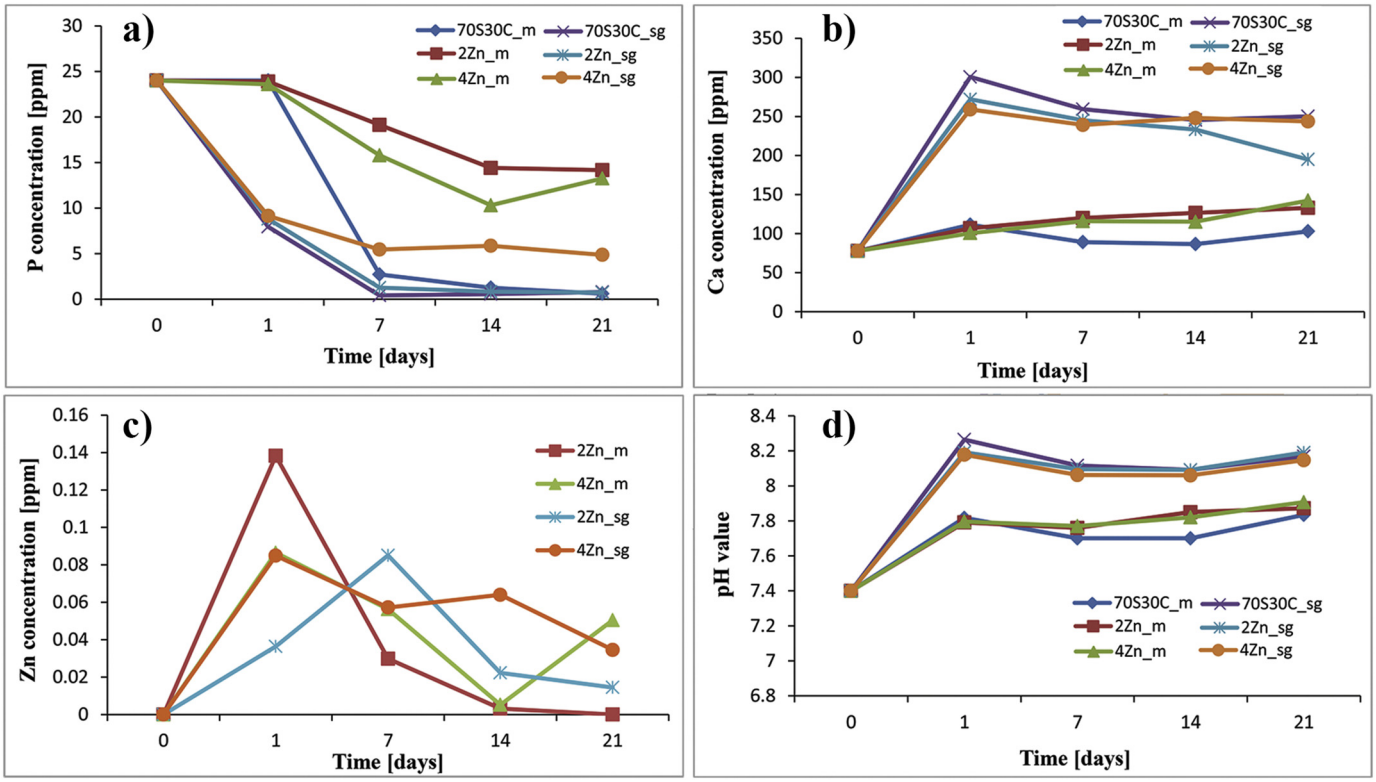


Fig. 7. Ion concentration: a) P, b) Ca, c) Zn and d) pH values of SBF containing the different bioactive glasses as function of time.

which correspond to the asymmetric bending vibrations of PO_4^{3-} groups [43] [33]. In the case of the zinc-doped melt-derived glasses these bands cannot be found, while spectra of 4Zn_sg has only one broad band at 560 cm^{-1}. Another extra band appears at about 962 cm^{-1} in the spectra of 70S30C_sg, which can be assigned to P—O stretching vibrations [44]. Furthermore, in the range 1415–1496 cm^{-1} arise bands, which correspond to the asymmetric stretching C—O vibrations in carbonate groups (CO_3^{2-}) [45] [46]. These measurements

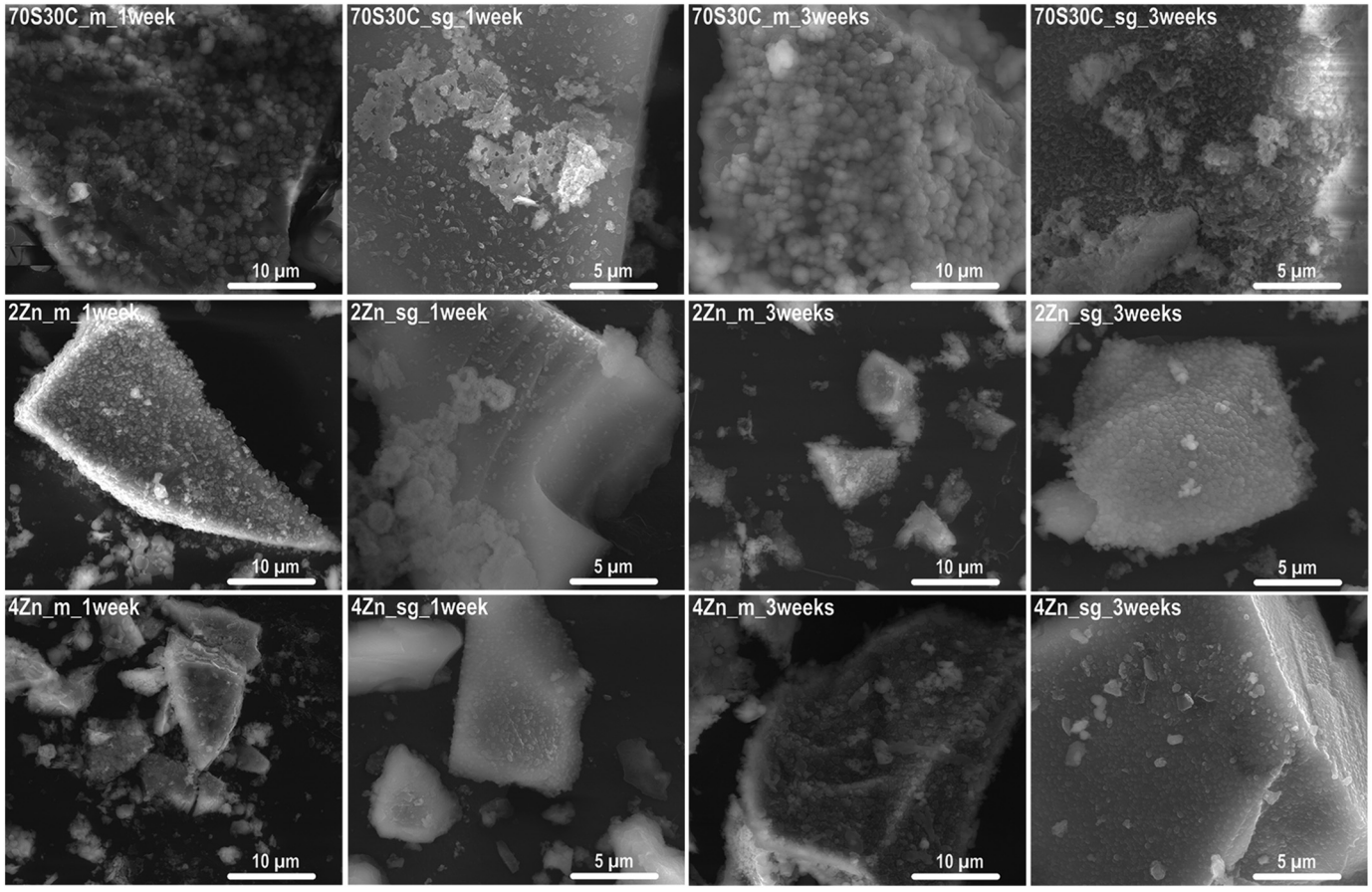


Fig. 8. SEM microphotographs of bioactive glass samples after 1 week and 3 weeks of incubation in SBF.

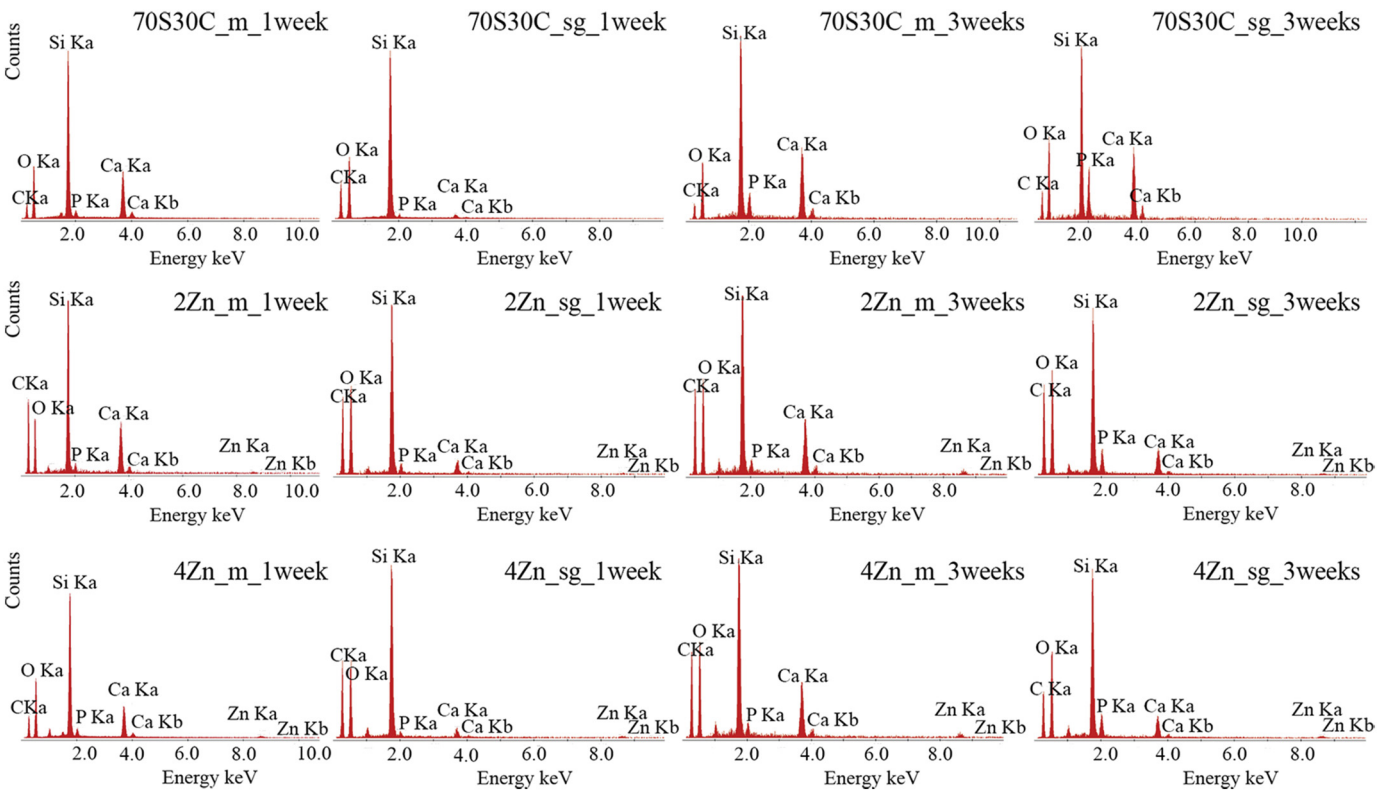


Fig. 9. EDX analysis after 1 week and 3 weeks of incubation in SBF showing increasing intensity of the P peak by increasing incubation time.

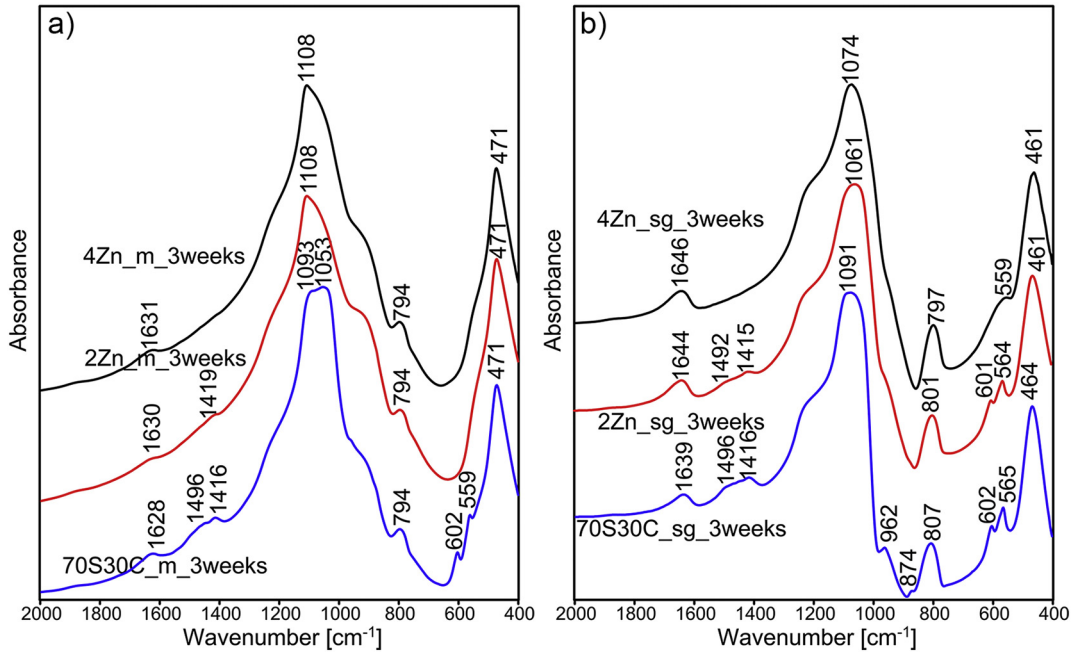


Fig. 10. MIR spectra of glasses surfaces after 3 weeks of incubation in SBF: a) melt-derived glasses, b) gel-derived glasses.

can confirm that with addition of zinc ion, the bioactivity decrease. In the case of 70S30C_m, 70S30C_sg and 2Zn_sg glasses, FTIR analysis may indicate that the newly created layer can be identified as carbonate-apatite because it comprises phosphate and carbonate groups.

To summarize the above-mentioned considerations, it is proposed that zinc ions inhibit the HCA layer formation due to their presence in the SBF solution.

3.7. In vitro biocompatibility

Cell morphology, number of attached cells (LDH activity) and cell viability (mitochondrial activity, WST) of osteoblast-like cells (MG-63 cells) were evaluated in accordance to the ISO 1993-5 biocompatibility test.

Fig. 11 presents the cell viability and LDH activity of MG-63 cells after cultivation time of 48 h. All samples show very high levels of cell mitochondrial activity (> 80% of the reference control). In general, a trend can be observed that zinc ions enhance the mitochondrial activity, as compared with 70S30C glasses. Statistically significant higher cell viability of cell population incubated in 1% concentration of 2Zn_m and 4Zn_m glasses was observed. It was also found that the MG-63 cells viability is affected by the method of glass preparation. The gel-derived samples exhibited statistically significant lower mitochondrial activity in comparison with their melt-derived equivalents. This effect can be associated with the higher pH values after dissolution of the gel-derived glasses.

On all samples, MG-63 cells showed similar level of LDH activity. Only the 4Zn_sg sample indicated statistically significant higher LDH activity of MG-63 cells in comparison with 70S30C_sg. This suggests that this material is slightly more favorable for cell proliferation.

The results indicate that all glasses are not cytotoxic (viability is always above 80%, which according to ISO 10993-5, indicates that the material should be considered as not cytotoxic [47]) and favorable for cell proliferation.

The morphology and the adhesion of MG-63 cells are presented in Fig. 12. The cells are seen to be spread and they fully covered the surface of the well-plates. The cells are elongated and of triangle shape, which is typical for healthy osteoblast-like cells. However in case of gel-derived glasses, the cells are found to be more round in shape, which can suggest that these glasses may have a negative impact on the cell metabolic activity, hindering their adhesion (as proven by the slightly lower viability results observed in the WST-8 study (Fig. 11a)). The observations of the cell morphology confirm the beneficial effect of zinc ions and non-toxic properties of all glasses.

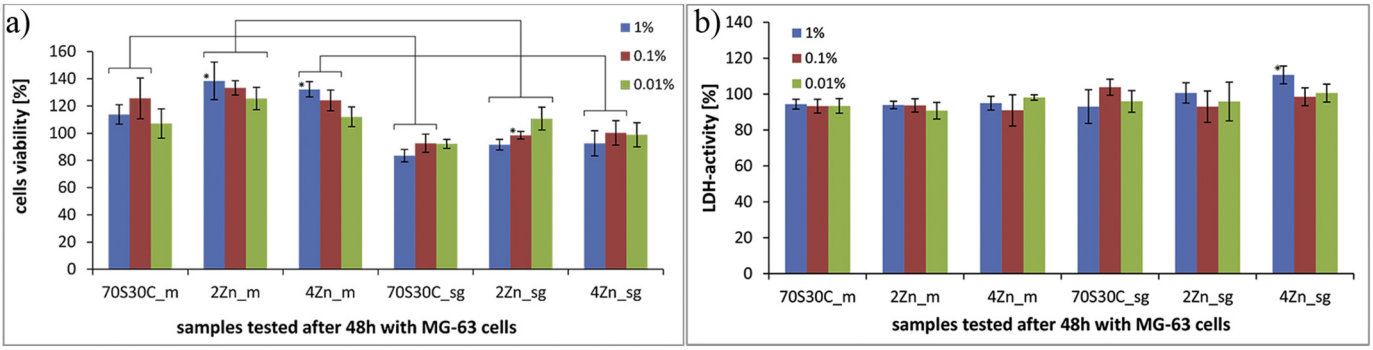


Fig. 11. a) cell viability and b) cell number (LDH activity) of samples tested after 48 h with MG-63. Asterisk (*) marks statistically significant differences ($p < .05$) between the zinc-modified and unmodified samples prepared by the same fabrication method. Significant differences between different fabrication method for the same chemical compositions are marked by brackets.

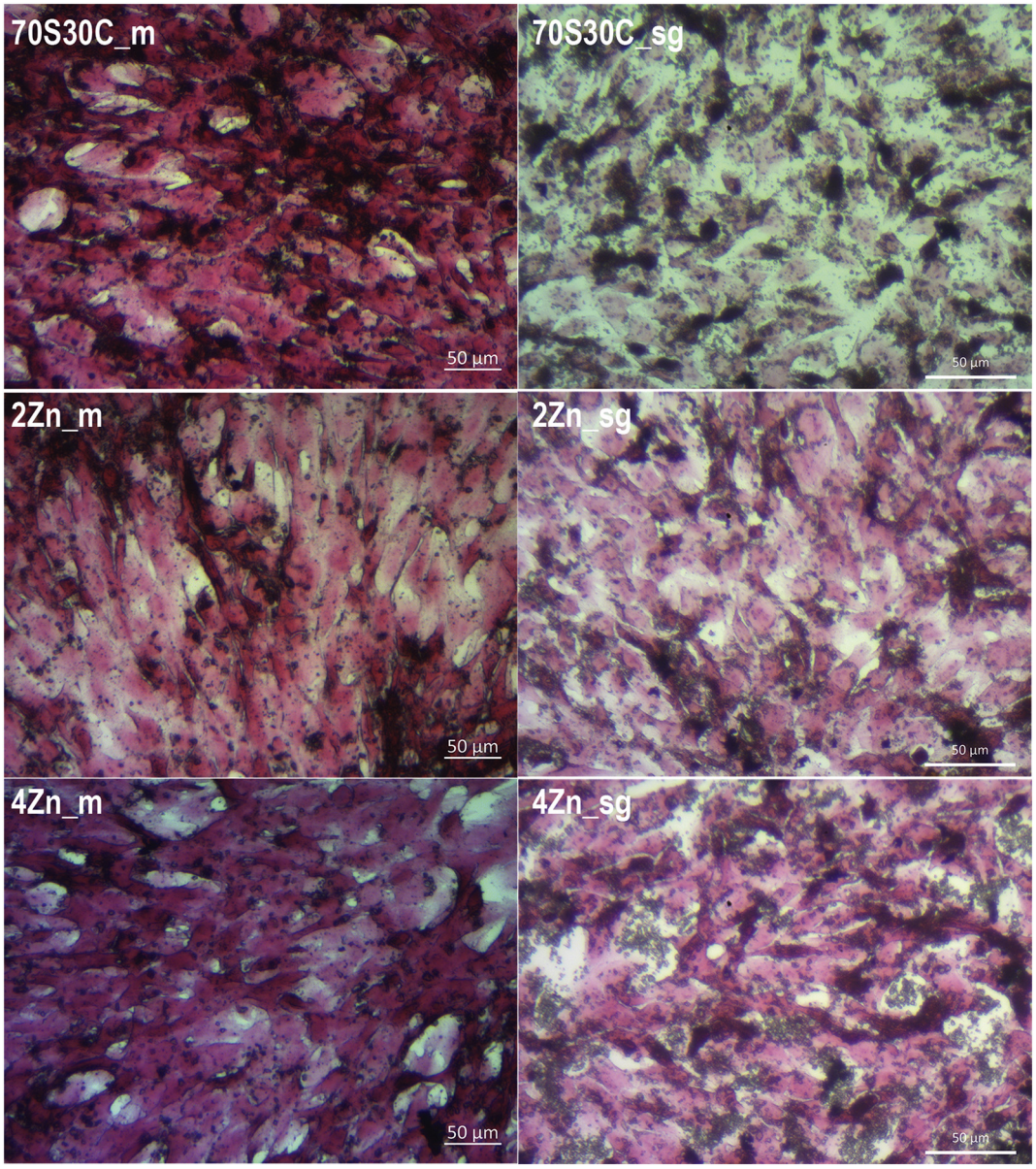


Fig. 12. Light microscope images showing morphology and adhesion of MG-63 cells after 48 h incubation.

Performed tests provide results that are indicative of material biocompatibility in contact with human osteoblast-like cells. Zinc ions enhance the cell viability and do not cause the reduction in cell number.

3.8. Antibacterial tests

Results of the comparative tests of antibacterial properties of zinc-doped glasses against gram-negative (*E. coli*) and gram-positive (*S. aureus*) bacteria are presented in Fig. 13. It can be observed that the 2Zn_m, 4Zn_sg and 70S30C_sg glasses, incubated with both concentrations of bacterial suspension, have a noticeable antibacterial effect towards the gram-positive -and negative bacteria. These results for zinc-doped glasses can be explained by the high concentration of zinc ions in water (at about 0.6 ppm – Fig. 7, the authors assumed that the trend of ion release in water can be similar to release in LB medium), which could increase bactericidal efficiency against the used bacteria. However the literature indicates that the mechanism of antibacterial effect can also be due to the presence of calcium ions [48] as well as the increase in the pH value [49]. In the case of the 4Zn_m glass, the zinc concentration in water after 24 h was the highest among all of the glasses, however this glass does not evoke antibacterial activity. This result may be the consequence of a lower Ca^{2+} concentration or the fact that excessive Zn^{2+} concentration can also favor growth of bacteria.

4. Conclusions

From our complete study of SiO_2-CaO glasses containing Zn, it can be concluded that zinc ions cause a decrease in specific pore volume and pore diameter. Structural analysis demonstrated that zinc ions play both roles: network modifier and network former, which lead to a decrease of glass transition temperature induced by weakening of the network (as revealed via FTIR and ^{29}Si MAS-NMR spectroscopy). During the incubation in the SBF, materials release the zinc ions. These may cause precipitation of some of the SBF compounds, hindering the formation of hydroxycarbonate apatite layer on the surface of the material. The obtained materials are not cytotoxic and zinc ions were seen to improve metabolic activity of MG-63 cells. In the study, an antibacterial effect of the zinc-modified and gel-derived glasses was revealed, as compared to unmodified and melted ones. This phenomenon is most likely attributed to higher concentration of Ca and Zn ions as

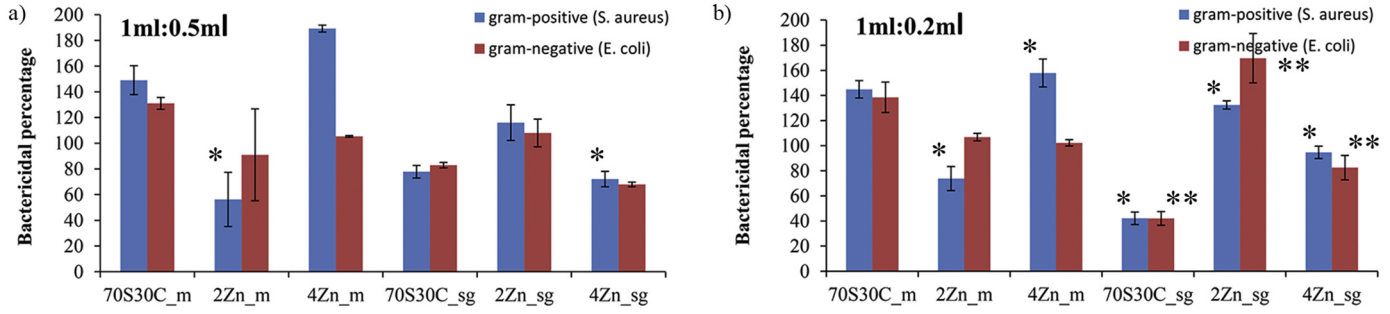


Fig. 13. The bactericidal percentages of different ratios of medium-sample extract to bacteria mixture: a) 1 ml:0.5 ml, b) 1 ml:0.2 ml). Asterisks mark statistically significant differences ($p < .05$) between the obtained glass and reference. * for gram-positive and ** for gram-negative.

well as higher pH. However, it was proven that this effect can only be obtained when a certain, optimal amount of ZnO is added to the sample. Thus, the present study confirms the necessity of careful designing of glass compositions in order to be able to evoke the desired reactions on both human and bacterial cells.

Acknowledgment

This work has been supported by the National Science Centre project no. 2016/20/T/ST8/00204,'Bioactive silico-phosphate glassy and glass-crystalline materials containing antibacterial ions'. W.H. Goldmann thanks the German Science Foundation (DFG, Go598) for it support. We thank Alina Grünewald for help in biocompatibility evaluation.

References

[1] L.L. Hench, J.K. West, Biological applications of bioactive glasses, Life Chem. Rep. 13 (1996) 187–241.
[2] A. Goel, S. Kapoor, R.R. Rajagopal, M.J. Pascual, H.-W. Kim, J.M.F. Ferreira, Alkali-free bioactive glasses for bone tissue engineering: A preliminary investigation, Acta Biomater. 8 (1) (2012) 361–372.
[3] G. Poologasundarampillai, D. Wang, S. Li, J. Nakamura, R. Bradley, P.D. Lee, M.M. Stevens, D.S. McPhail, T. Kasuga, J.R. Jones, Cotton-wool-like bioactive glasses for bone regeneration, *Acta Biomater.* 10 (8) (2014) 3733–3746.
[4] B. Zagrajczuk, M. Dziadek, Z. Olejniczak, K. Cholewa-Kowalska, M. Łączka, Structural and chemical investigation of the gel-derived bioactive materials from the SiO_2–CaO and SiO_2-CaO-P_2O_5 systems, *Ceram. Int.* 43 (15) (2017) 12742–12754.
[5] A. Martínez, I. Izquierdo-Barba, M. Vallet-Regí, Bioactivity of a CaO − SiO_2 Binary Glasses System, *Chem. Mater.* 12 (10) (2000) 3080–3088.
[6] S. Midha, T.B. Kim, W. Bergh, P.D. Lee, J.R. Jones, C.A. Mitchell, Preconditioned 70S30C bioactive glass foams promote osteogenesis in vivo, *Acta Biomater.* 9 (11) (2013) 9169–9182.
[7] A. Wajda, W.H. Goldmann, R. Detsch, A. Grünewald, A.R. Boccaccini, M. Sitarz, Structural characterization and evaluation of antibacterial and angiogenic potential of gallium-containing melt-derived and gel-derived glasses from CaO-SiO_2 system, *Ceram. Int.* 44 (18) (2018) 22698–22709.
[8] A. Moghanian, S. Firoozi, M. Tahriri, Characterization, in vitro bioactivity and biological studies of sol-gel synthesized SrO substituted 58S bioactive glass, *Ceram. Int.* 43 (17) (2017) 14880–14890.
[9] S.M. Rabiee, N. Nazparvar, M. Azizian, D. Vashaee, L. Tayebi, Effect of ion substitution on properties of bioactive glasses: A review, Ceram. Int. 41 (6) (2015) 7241–7251.
[10] A. Hoppe, N.S. Güldal, A.R. Boccaccini, A review of the biological response to ionic dissolution products from bioactive glasses and glass-ceramics, Biomaterials 32 (11) (2011) 2757–2774.
[11] L. Esteban-Tejeda, C. Prado, B. Cabal, J. Sanz, R. Torrecillas, J.S. Moya, Antibacterial and Antifungal Activity of ZnO Containing Glasses, PLoS ONE 10 (7) (2015) e0132709.
[12] I. Atkinson, E.M. Anghel, L. Predoana, O.C. Mocioiu, L. Jecu, I. Raut, C. Munteanu, D. Culita, M. Zaharescu, Influence of ZnO addition on the structural, in vitro behavior and antimicrobial activity of sol–gel derived CaO–P_2O_5–SiO_2 bioactive glasses, Ceram. Int. 42 (2) (2016) 3033–3045.
[13] M. Riaz, R. Zia, F. Saleemi, H. Ikram, F. Bashir, In vitro antimicrobial activity of ZnO based glass–ceramics against pathogenic bacteria, J. Mater. Sci. Mater. Med. 26 (12) (2015) 268.
[14] E. Saino, S. Grandi, E. Quartarone, V. Maliardi, D. Galli, N. Bloise, L. Fassina, M.G. De Angelis, P. Mustarelli, M. Imbriani, L. Visai, In vitro calcified matrix deposition by human osteoblasts onto a zinc-containing bioactive glass, Eur. Cell. Mater. 21 (2011) 59–72.
[15] V. Aina, A. Perardi, L. Bergandi, G. Malavasi, L. Menabue, C. Morterra, D. Ghigo, Cytotoxicity of zinc-containing bioactive glasses in contact with human osteoblasts, Chem. Biol. Interact. 167 (3) (2007) 207–218.
[16] S. Shahrabi, S. Hesaraki, S. Moemeni, M. Khorami, Structural discrepancies and in vitro nanoapatite formation ability of sol–gel derived glasses doped with different bone stimulator ions, Ceram. Int. 37 (7) (2011) 2737–2746.
[17] S. Kaya, M. Cresswell, A.R. Boccaccini, Mesoporous silica-based bioactive glasses for antibiotic-free antibacterial applications, Mater. Sci. Eng. C 83 (2018) 99–107.
[18] R. Pasqualini, C.F.B. Iii, W. Arap, Vessel maneuvers: Zinc fingers promote angiogenesis, Nat. Med. 8 (12) (2002) 1353–1354.
[19] Y.H. Cho, S.J. Lee, J.Y. Lee, S.W. Kim, C.B. Lee, W.Y. Lee, M.S. Yoon, Antibacterial effect of intraprostatic zinc injection in a rat model of chronic bacterial prostatitis, Int. J. Antimicrob. Agents 19 (6) (2002) 576–582.
[20] A.B.G. Lansdown, U. Mirastschijski, N. Stubbs, E. Scanlon, M.S. Ågren, Zinc in wound healing: Theoretical, experimental, and clinical aspects, Wound Repair Regen. 15 (1) (2007) 2–16.
[21] T.N. Phan, T. Buckner, J. Sheng, J.D. Baldeck, R.E. Marquis, Physiologic actions of zinc related to inhibition of acid and alkali production by oral streptococci in suspensions and biofilms, Oral Microbiol. Immunol. 19 (1) (2004) 31–38.
[22] J. Pasquet, Y. Chevalier, J. Pelletier, E. Couval, D. Bouvier, M.A. Bolzinger, The contribution of zinc ions to the antimicrobial activity of zinc oxide, Colloids Surf. A Physicochem. Eng. Asp. 457 (2014) 263–274.
[23] J. Román, S. Padilla, M. Vallet-Regí, Sol-gel glasses as precursors of bioactive glass ceramics, Chem. Mater. 15 (3) (2003) 798–806.
[24] M. Handke, W. Mozgawa, M. Nocuń, Specific features of the IR spectra of silicate glasses, J. Mol. Struct. 325 (1994) 129–136.
[25] T. Kokubo, H. Takadama, How useful is SBF in predicting in vivo bone bioactivity? Biomaterials 27 (15) (2006) 2907–2915.
[26] M. Tomozawa, V. McGahay, J.M. Hyde, Phase separation of glasses, J. Non-Cryst. Solids 123 (1990) 197–207.
[27] A. Wajda, M. Sitarz, Structural and microstructural comparison of bioactive melt-derived and gel-derived glasses from CaO-SiO_2 binary system, Ceram. Int. 44 (8) (2018) 8856–8863.
[28] M. Lubas, M. Sitarz, Z. Fojud, S. Jurga, Structure of multicomponent SiO_2–Al_2O_3–Fe_2O_3–CaO–MgO glasses for the preparation of fibrous insulating materials, *J. Mol. Struct.* 744-747 (2005) 615–619.
[29] M. Sitarz, The structure of simple silicate glasses in the light of Middle Infrared spectroscopy studies, J. Non-Cryst. Solids 357 (6) (2011) (1603–160).
[30] M. Sitarz, M. Rokita, M. Handke, E. Galuskin, Structural studies of the $NaCaPO_4$–SiO_2 sol–gel derived materials, *J. Mol. Struct.* 651–653 (2003) 489–498.
[31] C. Funaki, S. Yamamoto, H. Hoshina, Y. Ozaki, H. Sato, Three different kinds of weak C–H···O=C inter- and intramolecular interactions in poly(ε-caprolactone) studied by using terahertz spectroscopy, infrared spectroscopy and quantum chemical calculations, Polymer 137 (2018) 245–254.
[32] M. Sitarz, M. Handke, Z. Fojud, S. Jurga, Spectroscopic studies of glassy phosphosilicate materials, J. Mol. Struct. 744–747 (2005) 621–626.
[33] M. Dziadek, B. Zagrajczuk, E. Menaszek, A. Wegrzynowicz, J. Pawlik, K. Cholewa-Kowalska, Gel-derived SiO_2–CaO–P_2O_5 bioactive glasses and glass-ceramics modified by SrO addition, *Ceram. Int.* 42 (5) (2016) 5842–5857.6.
[34] M. Sitarz, Influence of modifying cations on the structure and texture of silicate–-phosphate glasses, *J. Mol. Struct.* 887 (1-3) (2008) 237–248.
[35] M. Sitarz, K. Bulat, M. Szumera, Influence of modifiers and glass-forming ions on the crystallization of glasses of the $NaCaPO_4$–SiO_2 system, J. Therm. Anal. Calorim. 109 (2) (2012) 577–584.
[36] J. Sułowska, I. Wacławska, M. Szumera, Comparative study of zinc addition effect on thermal properties of silicate and phosphate glasses, J. Therm. Anal. Calorim. 123 (2) (2016) 1091–1098.
[37] A. Wajda, M. Sitarz, Structural and microstructural studies of zinc-doped glasses from $NaCaPO_4$-SiO_2 system, J. Non-Cryst. Solids 441 (2016) 66–73.
[38] T.W.J. Albrecht, J. Addai-Mensah, D. Fornasiero, Effect of pH, Concentration and Temperature on Copper and Zinc Hydroxide Formation/Precipitation in Solution, Chemeca, Engineering a Better World, Sydney (2011).
[39] G. Kaur, G. Pickrell, G. Kimsawatde, D. Homa, H.A. Allbee, N. Sriranganathan, Synthesis, cytotoxicity, and hydroxyapatite formation in 27-Tris-SBF for sol-gel based CaO-P_2O_5-SiO_2-B_2O_3-ZnO bioactive glasses, Sci. Rep. 4 (2014).
[40] M. Vallet-Regí, Ceramics for medical applications, J. Chem. Soc. Dalton Trans. (2) (2001) 97–108.

[41] A. Moghanian, S. Firoozi, M. Tahriri, Synthesis and in vitro studies of sol-gel derived lithium substituted 58S bioactive glass, *Ceram. Int.* 43 (15) (2017) 12835–12843.
[42] D.B. Jaroch, D.C. Clupper, Modulation of zinc release from bioactive sol–gel derived SiO_2-CaO-ZnO glasses and ceramics, J. Biomed. Mater. Res. A 82A (3) (2007) 575–588.
[43] W. Jastrzębski, M. Sitarz, M. Rokita, K. Bułat, Infrared spectroscopy of different phosphates structures, Spectrochim. Acta A Mol. Biomol. Spectrosc. 79 (4) (2011) 722–727.
[44] M. Todea, R.V.F. Turcu, B. Frentiu, S. Simon, FTIR and NMR evidence of aluminosilicate microspheres bioactivity tested in simulated body fluid, J. Non-Cryst. Solids 432 (2016) 413–419.
[45] J. Chen, L. Zeng, X. Chen, T. Liao, J. Zheng, Preparation and characterization of bioactive glass tablets and evaluation of bioactivity and cytotoxicity in vitro, Bioact. Mater. 3 (3) (2018) 315–321.
[46] S.L. Aktuğ, S. Durdu, E. Yalçın, K. Çavuşoğlu, M. Usta, Bioactivity and biocompatibility of hydroxyapatite-based bioceramic coatings on zirconium by plasma electrolytic oxidation, Mater. Sci. Eng. C 71 (C) (2017) 1020–1027.
[47] ISO 10993-5:2009 (E), Biological evaluation of medical devices - Part 5: Tests for in Vitro Cytotoxicity, International Organization for Standardization, (2009).
[48] D. Khvostenko, T.J. Hilton, J.L. Ferracane, J.C. Mitchell, J.J. Kruzic, Bioactive glass fillers reduce bacterial penetration into marginal gaps for composite restorations, Dent. Mater. 32 (1) (2016) 73–81.
[49] S. Hu, J. Chang, M. Liu, C. Ning, Study on antibacterial effect of 45S5 Bioglass, J. Mater. Sci. Mater. Med. 20 (1) (2009) 281–286.